The type IV pilin PilA couples surface attachment and cell cycle initiation in *Caulobacter crescentus*

Luca Del Medico[a], **Dario Cerletti**[a], **Matthias Christen**[a,1], **and Beat Christen**[a,1]

[a]Institute of Molecular Systems Biology, Department of Biology, ETH Zürich, Zurich, Switzerland

This manuscript was compiled on September 11, 2019

Understanding how bacteria colonize surfaces and regulate cell cycle progression in response to cellular adhesion is of fundamental importance. Here, we used transposon sequencing in conjunction with FRET microscopy to uncover the molecular mechanism how surface sensing drives cell cycle initiation in *Caulobacter crescentus*. We identified the type IV pilin protein PilA as the primary signaling input that couples surface contact to cell cycle initiation via the second messenger c-di-GMP. Upon retraction of pili filaments, the monomeric pilin reservoir in the inner membrane is sensed by the 17 amino-acid transmembrane helix of PilA to activate the PleC-PleD two component signaling system, increase cellular c-di-GMP levels and signal the onset of the cell cycle. We termed the PilA signaling sequence CIP for cell cycle initiating pilin peptide. Addition of the chemically synthesized CIP peptide initiates cell cycle progression and simultaneously inhibits surface attachment. The broad conservation of the type IV pili and their importance in pathogens for host colonization suggests that CIP peptide mimetics offer new strategies to inhibit surface-sensing, prevent biofilm formation and control persistent infections.

Caulobacter crescentus | c-di-GMP | Type IV pilin | TnSeq | FRET microscopy

The cell cycle model bacterium *Caulobacter crescentus* (*Caulobacter* thereafter) integrates surface colonization into a bi-phasic life-cycle. Attachment begins with a reversible phase, mediated by surface structures such as pili and flagella, followed by a transition to irreversible attachment mediated by polysaccharides (1–4). In *Caulobacter* surface sensing is intimately interlinking with cellular differentiation and cell cycle progression (5, 6). During the bi-phasic life cycle, *Caulobacter* divides asymmetrically and produces two distinct cell types with specialized development programs (Fig. 1a). The sessile stalked cell immediately initiates a new round of chromosome replication, whereas the motile swarmer cell, equipped with a polar flagellum and polar pili, remains in the G1 phase for a defined interval before differentiating into a stalked cell and entering into the replicative S phase driven by the second messenger c-di-GMP dependent degradation of the cell cycle master regulator CtrA (7, 8) (Fig. 1a). The change in cell cycle state from motile swarmer into surface attached replication-competent stalked cells depends on tactile sensing mechanisms. Both pili and flagella have been previously implicated as key determinants involved in tactile surface sensing (9, 10). However, understanding the molecular mechanism of how *Caulobacter* interlinks bacterial surface attachment to cell cycle initiation has remained elusive.

In this work, we report on a short peptide signal encoded within the type IVb pilin protein PilA that exerts pleiotropic control and links bacterial surface attachment to cell cycle initiation in *Caulobacter*. Using FRET microscopy in conjunction with a genetically encoded c-di-GMP biosensor (11), we quantify c-di-GMP signalling dynamics inside single cells and found that, besides its structural role in forming type IVb pili filaments, monomeric PilA in the inner membrane functions as a specific input signal that triggers c-di-GMP signalling at the G1-S phase transition.

Results

A specific cell cycle checkpoint delays cell cycle initiation. To understand how bacterial cells adjust the cell cycle to reduced growth conditions, we profiled the replication time of the α-proteobacterial cell cycle model organism *Caulobacter* across the temperature range encountered in its natural freshwater habitat (Table S1). Under the standard laboratory growth temperature of 30°C, *Caulobacter* replicates every 84 ± 1.2 min. However, when restricting the growth temperature to 10°C, we observed a 13-fold increase in the duration of the cell cycle, extending the replication time to 1092 ± 14.4 min (Table S1). To investigate whether reduced growth resulted in a uniform slow-down or affects particular cell cycle phases, we determined the relative length of the G1 phase by fluorescence microscopy using a previously described cell cycle reporter strain (11) (Materials and Methods). We found that the culturing of *Caulobacter* at 10°C caused a more than 1.4-fold increase in the relative duration of the G1 phase indicating a delay in cell cycle initiation (Fig. 1b). This finding suggested the presence of a specific cell cycle checkpoint that delays cell cycle initiation during reduced growth conditions.

Significance Statement

Pili are hair-like appendages found on the surface of many bacteria to promote adhesion. Here, we provide systems-level findings on a molecular signal transduction pathway that interlinks surface sensing with cell cycle initiation. We propose that surface attachment induces depolymerization of pili filaments. The concomitant increase in pilin sub-units within the inner membrane function as a stimulus to activate the second messenger c-di-GMP and trigger cell cycle initiation. Furthermore, we show that the provision of a 17 amino acid synthetic peptide corresponding to the membrane portion of the pilin sub-unit mimics surface sensing, activates cell cycle initiation and inhibits surface attachment. Thus, synthetic peptide mimetics of pilin may represent new chemotypes to control biofilm formation and treat bacterial infections.

LDM, MC, and BC conceived the research; LDM performed transposon mutagenesis experiments, LDM perfomed FRET microscopy, DC performed time-lapse FRET microscopy; LDM, MC, and BC analyzed data; LDM, MC, and BC wrote the manuscript.

No conflict of interest declared.

[1]To whom correspondence should be addressed. E-mail: matthias.christen@imsb.biol.ethz.ch; beat.christen@imsb.biol.ethz.ch

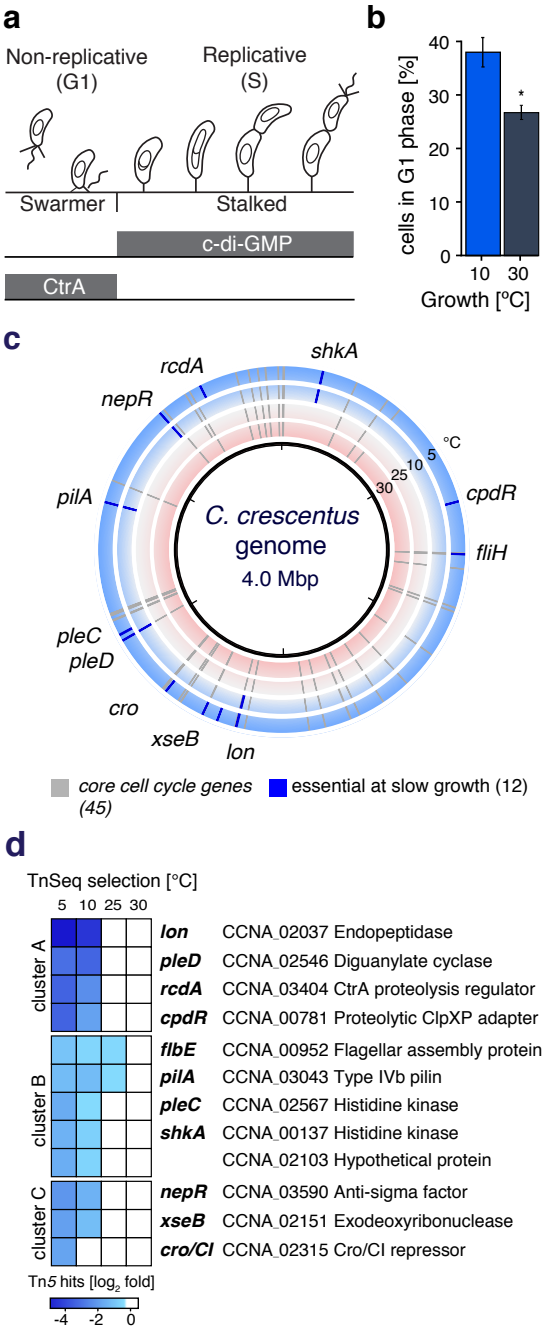

Fig. 1. Transposon sequencing identifies conditionally essential genes required during reduced growth. (a) *Caulobacter* divides asymmetrically into a replication competent stalked cell and a swarmer cell. The master regulator CtrA inhibits DNA replication in swarmer cells and is proteolytically cleared upon an increase in cellular levels of the second messenger c-di-GMP at the G1-S phase transition. **(b)** Cellular replication under slow-growth conditions increases the relative duration of the G1-phase. **(c)** TnSeq across the 4.0 Mbp *Caulobacter* genome defines 45 core-essential cell cycle genes (grey marks) to sustain growth at 5℃, 10℃, 25℃ and 30℃ (outer to inner track) and 12 conditionally essential genes required for slow-growth conditions (blue marks). **(d)** Hierarchical cluster analysis of the 12 conditionally essential genes required for slow growth.

TnSeq identifies conditionally essential cell cycle genes. To identify the complete set of genes required for cell cycle progression at different growth rates, we designed a systems-wide forward genetic screen based on quantitative selection analysis coupled to transposon sequencing (TnSeq) (12, 13). TnSeq measures genome-wide changes in transposon insertion abundance upon subjecting large mutant populations to different selection regimes and enables genome-wide identification of essential genes. We hypothesised that the profiling of growth-rate dependent changes in gene essentiality will elucidate the components of the cell cycle machinery fundamental for cell cycle initiation under reduced growth conditions. We selected *Caulobacter* transposon mutant libraries for prolonged growth at low temperatures (5°C and 10°C) and under standard laboratory cultivation conditions (25°C and 30°C). Cumulatively, we mapped for each condition between 397'377 and 502'774 unique transposon insertion sites across the 4.0 Mbp *Caulobacter* genome corresponding to a transposon insertion densities of 4-5 bp (Table S2).

To identify the factors required for cell cycle progression, we focused our analysis on essential genes (Data SI) that are expressed in a cell cycle-dependent manner (Materials and Methods, (14–16)). Among 373 cell cycle-controlled genes, we found 45 genes that were essential under all growth conditions (Fig. 1c, Data SI), including five master regulators (*ctrA*, *gcrA*, *sciP*, *ccrM* and *DnaA*), eleven divisome and cell wall components (*ftsABILQYZ*, *fzlA* and *murDEF*), six DNA replication and segregation factors (*dnaB*, *ssb*, *gyrA*, *mipZ*, *parB* and *ftsK*) as well as 23 genes encoding for key signalling factors and cellular components required for cell cycle progression (Data SI). Collectively, these 45 genes form the core components of the bacterial cell cycle machinery.

Components of the c-di-GMP signalling network are conditionally essential for slow growth. During reduced growth conditions, we found 12 genes that specifically became essential (Fig. 1c). To gain insights into the underlying genetic modules, we performed a hierarchical clustering analysis and grouped these 12 genes according to their growth-rate dependent fitness profile into three functional clusters A, B and C (Fig. 1d, Materials and Methods).

Cluster A contained four conditionally essential genes that exhibited a large decrease in fitness during slow-growth conditions (Fig 1d, Fig. S1). Among them were *pleD*, *cpdR*, *rcdA* and *lon* that all comprise important regulators for cell cycle controlled proteolysis. The diguanylate cyclase PleD produces the bacterial second messenger c-di-GMP, which becomes restricted to the staked cell progeny upon asymmetric cell division and is absent in the newly born swarmer cell (Fig. 1a, (17)). During the G1-S phase transition, c-di-GMP levels raise again and trigger proteolytic clearance of the cell cycle master regulator CtrA (Fig 1a), which is mediated by ClpXP and the proteolytic adaptor proteins RcdA, CpdR and PopA (18–20). Similarly, the ATP-dependent endopeptidase Lon is responsible for the degradation of the cell cycle master regulators CcrM, DnaA and SciP (21–23). Taken together, these findings underscore the importance to control proteolysis of CtrA and other cell cycle regulators to maintain cell cycle progression at low growth rates when intrinsic protein turnover rates are marginal.

Cluster B contained five genes including the two kinase genes *pleC* and *shkA*, a gene of unknown function encoding for a conserved hypothetical protein (CCNA_02103) as well as the type IV pilin gene *pilA* and the flagellar assembly ATPase *flbE/fliH* (Fig 1d, Fig. S2). Multiple genes of cluster B par-

ticipate in c-di-GMP signalling. Among them, we found the sensor kinase PleC that functions upstream and activates the diguanylate cyclase PleD over phosphorylation. The hybrid kinase ShkA comprises a downstream effector protein of PleD, which binds c-di-GMP and phosphorylates the TacA transcription factor responsible for the initiation of the stalked-cell specific transcription program (24). The flagellum assembly ATPase FlbE/FliH together with FliI and FliJ form the soluble component of the flagellar export apparatus, which in *Pseudomonas* has also been identified as a c-di-GMP effector complex (25). Collectively, these data indicate that c-di-GMP signalling is of fundamental importance to coordinate cell cycle progression under slow-growth conditions.

Cluster C comprised the anti-sigma factor *nepR*, a Cro/CI transcription factor (CCNA_02315) and *xseB* encoding the small subunit of the exodeoxyribonuclease VII (Fig 1d, Fig. S3), which form outer-circle components not directly linked to c-di-GMP signalling. However, disruption of these genes likely induces stress response and alternative transcriptional programs that may interfere with cell cycle progression under slow-growth conditions.

PilA induce c-di-GMP signalling. Among the components of the c-di-GMP signalling network identified within cluster A and B, the sensor kinase PleC resides at the top of the signalling hierarchy activating the diguanylate cyclase PleD at the G1-S phase transition. While the activation mechanism of its down stream target PleD has been resolved with molecular detail (26), the type of external signal integrated by PleC has remained unknown. PleC comprises an amino-terminal periplasmic domain, which suggests that PleC activity is controlled by an external signal. Among the identified conditionally essential gene within cluster B, PilA co-clustered together with PleC (Fig 1d). The Type IV pilin protein PilA is translocated into the periplasm and shares the same sub-cellular localization pattern to the swarmer specific cell pole as PleC (17, 27). Thus, we speculated that PilA is a likely candidate for the hitherto unknown external input signal perceived by the sensor kinase PleC.

To test this hypothesis, we monitored the c-di-GMP signalling dynamics in a wildtype and Δ*pilA* background. The activation of PleC, and subsequently PleD, leads to a strong increase in the c-di-GMP levels at the G1-S phase transition (Fig. 1a, (11)). Any mutation that impairs activation of PleC is expected to prolong the G1-swarmer phase. To monitor c-di-GMP signalling dynamics inside single cells, we have previously engineered a genetically encoded FRET-biosensor that permits time-resolved monitoring of the fluctuating c-di-GMP levels along the cell cycle (17). We synchronized wildtype and Δ*pilA* cells expressing this FRET biosensor and quantified c-di-GMP levels in individual swarmer cells by FRET-microscopy (Fig. 2a, Materials and Methods). In the wildtype control, we observed that the majority of synchronized cells quickly transitioned into the S phase with only 11.8% (143 out of 1073 cells) remaining in the G1 phase as indicated by low c-di-GMP levels (Fig. 2a,b). In contrast, we observed that more than 52.2% (821 out of 1570 cells) of all synchronized Δ*pilA* mutant cells exhibited a delay in the G1-S transition and maintained low c-di-GMP levels for a prolonged interval (Fig. 2a,b). Similarly, using time-lapse studies to follow signalling trajectories of individual cells, we found that Δ*pilA* mutants exhibited a more than 1.8 fold increase in the duration of the G1 phase as compared to wildtype cells (Fig. 2c). Providing a episomal copy of *pilA* restored the cell cycle timing defect of a Δ*pilA* mutant strain (Fig. 2a,b). These findings establish the type IV pilin PilA as a novel cell cycle input signal.

PilA controls cell cycle initiation via the sensor kinase PleC and the diguanylate cyclase PleD. PleC is a bifunctional phosphatase/kinase that switches activity in a cell cycle dependent manner (28). In the newborn swarmer cell, PleC first assumes phosphatase activity to inactivate the diguanylate cyclase PleD and establish low cellular c-di-GMP levels. Subsequently, PleC switches to a kinase and activates PleD at the G1-S-phase transition. To test whether PilA functions as an input signal for the PleC-PleD signalling cascade, we measured c-di-GMP signalling dynamics and compared the duration of the G1 phase in single and double deletion mutants using FRET microscopy (Materials and Methods, Fig. S4). Similar to Δ*pilA* mutants, Δ*pleD* mutants also prolonged the G1 phase more than two-fold as compared to the wildtype control (18% and 22% versus 9% G1 cells in wildtype, Fig. S4). However, a Δ*pilA*, Δ*pleD* double mutant only marginally increased the duration of the G1 phase and showed similar frequencies of swarmer cells with low-c-di-GMP levels as compared to a strain lacking solely *pleD* (28% and 22% G1 cells, Fig S4). This genetic evidence suggest that PilA resides upstream of PleD. Thus, besides its role as a structural component of the type IVb pilus, PilA likely comprises an input signal for the sensor kinase PleC, which serves as the cognate kinase of PleD, to increase c-di-GMP levels at the G1-S phase transition.

The inner membrane reservoir of the type IV pilin PilA signals cell cycle initiation. PilA harbours a short 14 aa N-terminal leader sequence required for translocation across the inner membrane that is cleaved off by the peptidase CpaA (29–31). To test whether translocation of PilA is a prerequisite for signalling the cell cycle initiation, we constructed a cytosolic version of PilA ($pilA_{15\text{-}59}$) lacking the N-terminal leader sequence needed for the translocation of the matured PilA across the membrane. Unlike the full-length PilA, the episomal expression of the translocation-deficient version of PilA did not complement for the cell cycle timing defect of a Δ*pilA* mutant. Similarly, we found that solely expressing the N-terminal leader sequence of PilA ($pilA_{1\text{-}14}$) neither restored the cell cycle timing defects of a Δ*pilA* mutant (Fig. 2d, Fig. S5, Table S3). We concluded that the translocation of PilA into the periplasm is a prerequisite to signal cell cycle initiation.

Upon translocation and cleavage of the N-terminal leader sequence, the mature form of PilA resides as a monomeric protein in the inner membrane (32). Through the action of a dedicated type IV pilus assembly machinery, the inner membrane-bound reservoir of PilA polymerizes into polar pili filaments that mediate initial attachment to surfaces (33). However, only *pilA* but none of the other component of the pilus assembly machinery became essential in our TnSeq screen under slow-growth conditions (Fig. 1c, Table S4, Data SI). Furthermore, unlike Δ*pilA* mutants, deletion mutants of the pilus assembly machinery genes *cpaA*, *cpaD*, and *cpaE* did not prolong the G1 phase but, in contrast, shorted the duration of the G1-phase two-fold as compared to the wildtype control (4%, 3%, and 5% G1 cells, Fig S4). The observation that the translocation of PilA monomers across the inner membrane is necessary but the subsequent polymerization of PilA

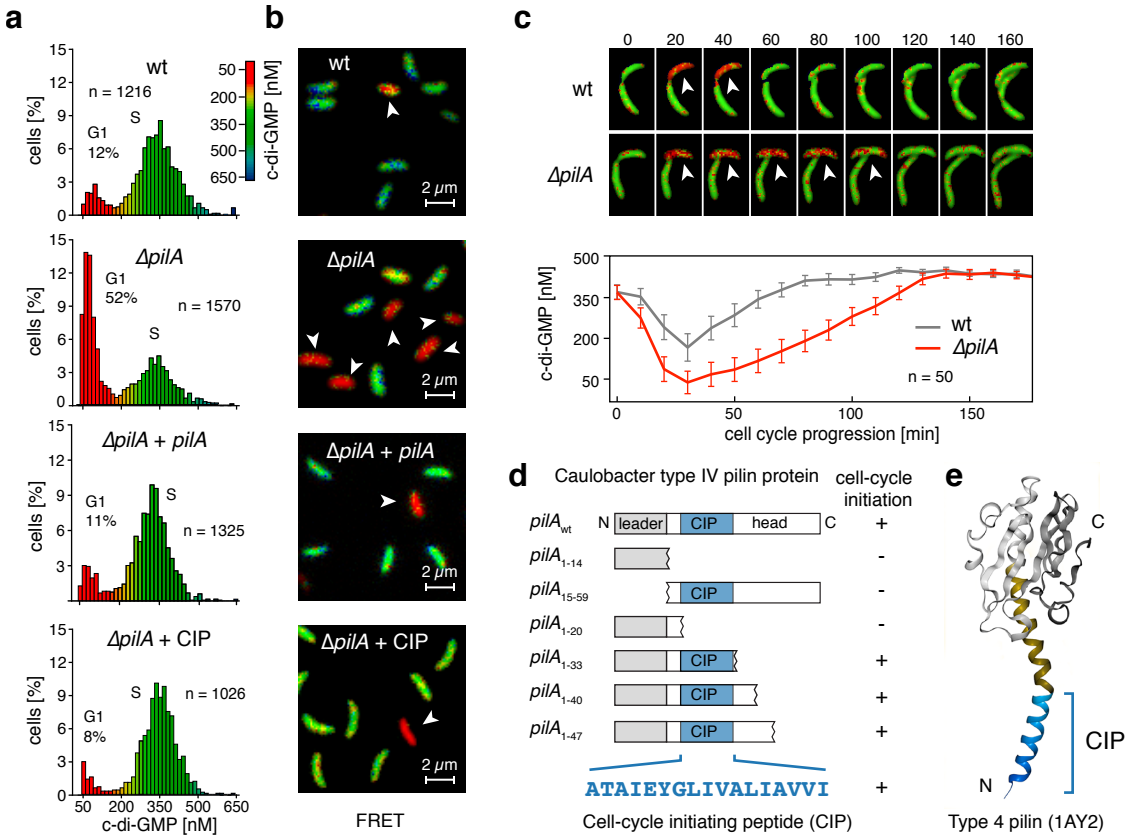

Fig. 2. The CIP sequence encoded in the N-terminal portion of PilA functions as cell cycle initiating signal. (a) Population distribution of intra-cellular c-di-GMP concentrations in synchronized *Caulobacter* cells. The population shows a bimodal c-di-GMP distribution corresponding to swarmer cells (G1) prior and after (S) the G1 to S transition. **(b)** (Top) Dual-emission ratio microscopic (FRET) images of synchronized swarmer populations of wild-type *Caulobacter*, Δ*pilA* mutants Δ*pilA* complemented by a plasmid born copy of *pilA* and Δ*pilA* complemented by the exogenous addition of cell cycle initiating peptide CIP (100 uM). Pseudocolors show FRET emission ratios (527/480 nm) corresponding to the cytoplasmic c-di-GMP concentration as indicated by the color bar. Swarmer cells (highlighted by arrows) resting in the G1 phase prior initiation of cell cycle exhibit low cellular c-di-GMP levels. **(c)** Kinetics of fluorescence ratio changes (527/480 nm), reflecting c-di-GMP levels recorded in *Caulobacter* cells during the S to G1 transition. Upper panel: Time-lapse dual-emission ratiometric FRET microscopy of representative cells of *Caulobacter* wild-type (wt) and Δ*pilA* mutants recorded at intervals of 10 min. Lower panel: Corresponding plots of the measured c-di-GMP fluctuations for the indicated strains over time. The average single cell FRET ratio over a population of 50 cells upon cell division is shown for wild type (grey) and Δ*pilA* (red). The drop in c-di-GMP levels is larger and sustained much longer for the Δ*pilA* mutant. **(d)** Complementation of the cell cycle initiation defect of Δ*pilA* with a panel of N- and C-terminal truncated PilA variants. **(e)** The CIP peptide sequence is modeled onto the type IV pilin from *Neisseria* that harbours a larger globular C-terminal domain (grey) which is absent in the *Caulobacter* PilA protein (gold).

monomers into mature pilin filaments is dispensable for cell cycle initiation, suggested that the periplasmic membrane reservoir of the monomeric form of PilA functions as an input signal for c-di-GMP mediated cell cycle signalling.

The trans-membrane helix of PilA comprises a 17 amino-acid peptide signal that mediates cell cycle initiation. The mature form of PilA is a small 45 aa protein comprised of a highly hydrophobic N-terminal alpha-helix (α1N), which anchors PilA in the inner membrane (30, 32), and an adjacent variable alpha-helical domain protruding into the periplasm. To identify the portion of the matured PilA protein responsible for triggering cell cycle initiation, we constructed a panel of C-terminally truncated *pilA* variants and assessed their ability to complement the cell cycle defect of a chromosomal *ΔpilA* mutant by quantifying c-di-GMP dynamics in single cells using FRET-microscopy (Materials and Methods). The expression of a truncated PilA variant that includes the leader sequence and the first 5 N-terminal amino-acids of the matured PilA protein ($pilA_{1\text{-}20}$) did not complement the cell cycle initiation defect of a *ΔpilA* mutant (Fig. 2d, Fig. S5, Table S3). However, increasing the N-terminal portion of the matured PilA protein to 17, 25, and 37 amino acids ($pilA_{1\text{-}33}$, $pilA_{1\text{-}40}$, $pilA_{1\text{-}47}$) restored the cell cycle initiation defects of a *ΔpilA* mutant (Fig. 2d, Fig. S5, Table S3). Based on these findings, we concluded that a small N-terminal peptide sequence covering only 17 N-terminal amino acids from the mature PilA (Fig. 2e) is sufficient to initiate c-di-GMP dependent cell cycle progression. Accordingly, we annotated these 17 amino acids as cell cycle initiating pilin sequence (CIP) (Fig. 2e).

Chemically synthesized CIP peptide initiates cell cycle progression. Next, we asked whether the translocation of PilA from the cytoplasm into the inner membrane or the presence of a PilA reservoir in the periplasm is sensed. If signalling depends solely on the presence of membrane inserted PilA, we speculated that exogenous provision of chemical-synthesized CIP peptide should restore the cell cycle defects in a *ΔpilA* mutant. To test this hypothesis, we incubated synchronized swarmer cells of a *ΔpilA* mutant in the presence of 100μM

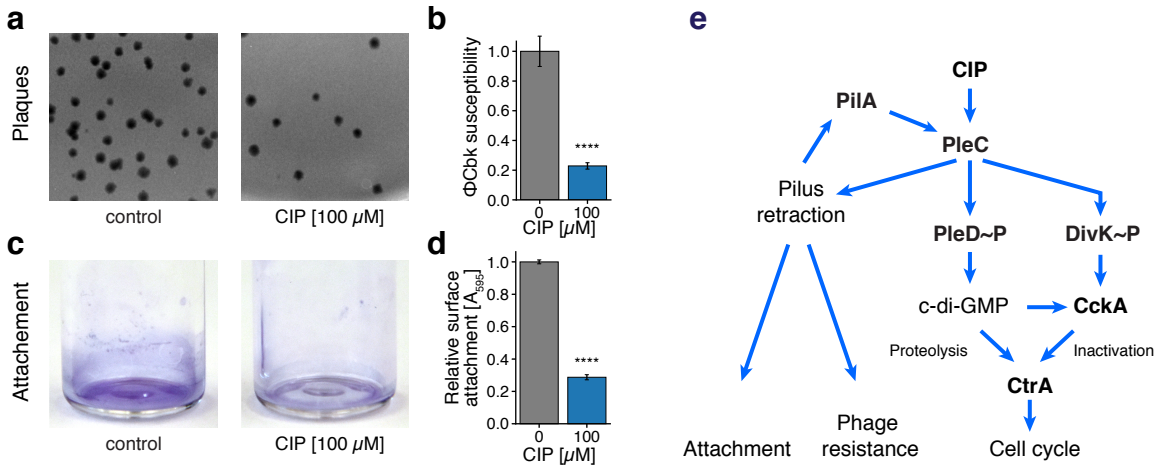

Fig. 3. Pleotropic effects and proposed mode of action of the cell cycle initiating pilin peptide (CIP). (a) ΦCbk phage susceptibility assay of *Caulobacter* CB15 in the presence (right panel) and absence (left panel) of 100 µM CIP as detected by the formation of plaques on double agar overlay (n= 5). **(b)** Corresponding bargraph plot of the relative ΦCbk phage susceptibility of *Caulobacter* CB15 upon 10 min of incubation without (n = 5) or with (n = 5) 100 µM CIP peptide. Error bars = s.e.m., ****: P << 10^{-4}. **(c)** Crystal violet surface attachment assay of *Caulobacter* CB15 in the presence (right panel) and absence (left panel) of 100 µM CIP. **(d)** Corresponding bargraph plot of the relative surface attachment of *Caulobacter* CB15 upon 1 h of incubation without (n = 9) or with (n = 9) 100 µM CIP peptide. Error bars = s.e.m., ****: P << 10^{-4}. **(e)** Model for the mode of action of the CIP peptide. The kinase activity of the pleiotropic, membrane bound sensor kinase PleC is activated by the CIP peptide mimicking a inner membrane reservoir of PilA monomers. The CIP peptide modulates PleC activity to promote phosphorylation of the downstream effectors PleD and DivK as well as activates pili retraction as part of a positive feedback loop. CtrA activity must be removed from cells at the onset of DNA replication, because phosphorylated CtrA binds to and silences the origin of replication. The c-di-GMP and CckA signalling cascade orchestrates cell cycle entry through controlled proteolysis and inactivation of the master cell cycle regulator CtrA.

of chemically synthesized CIP peptide and assayed c-di-GMP signalling dynamics by FRET microscopy (Fig. 2a,b). Indeed, we found that addition of the CIP peptide induced cell cycle transition into the S-phase as indicated by a 6.5 fold lower abundance of G1-swarmer cells with low c-di-GMP levels as compared to an untreated *ΔpilA* cell population (8% vs 52% G1 cells, Fig. 2a,b). These findings suggest that the addition of the CIP peptide shortens the G1 phase and, thus, functions as a cell cycle activator. Collectively, these result demonstrated that neither the translocation or polymerization but solely the inner membrane reservoir of PilA is sensed via the hydrophobic CIP sequence to initiate cell cycle progression.

The CIP peptide reduces surface attachment and ΦCbk phage susceptibility. Deletion of the sensor kinase *pleC* results in pleiotrophic defects and causes daughter cells to omit the G1-phase with low c-di-GMP levels (Fig. S4, (17)). Furthermore, *pleC* deletion mutants lack polar pili and show defects in initial attachment to surfaces (34). The observation that the addition of the CIP peptide shortens the G1-phase, suggests that the CIP sequence of PilA modulates PleC activity to promote phosphorylation of the downstream effector PleD. To test this hypothesis, we investigated whether the addition of the chemically synthesized CIP peptide also impairs additional PleC-specific output functions. Indeed, when assaying for the presence of functional pili using pili-specific bacteriophage CbK, we found that the incubation of synchronized wildtype *Caulobacter* for 10 min with the CIP peptide resulted in a 77.2 ± 2.1% decrease in bacteriophage CbK susceptibility (Fig. 3a,b), suggesting that CIP impairs pili function. Furthermore, we also found that the addition of the CIP peptide to wildtype *Caulobacter CB15* cells reduced initial attachment by 71.3 ± 1.6% (Fig. 3c,d) with a half-effective peptide concentration (EC_{50}) of 8.9 µM (Fig. S6) and a Hill coefficient of 1.6 suggesting positive cooperativity in binding of CIP to a multimeric receptor complex. Altogether, these findings support a model in which the CIP sequence of PilA functions as a pleiotropic small peptide modulator of the sensor kinase PleC leading to premature cell cycle initiation, retraction of type IV pili and impairment of surfaces attachment.

Discussion

Understanding how bacteria regulate cell cycle progression in response to external signalling cues is of fundamental importance. In this study, we used a transposon sequencing approach to identify genes required for cell cycle initiation. Comparing deviations in gene essentiality between growth at low temperatures (5°C and 10°C) and under standard laboratory cultivation conditions (25°C and 30°C) allowed us to pinpoint genes required exclusively for cell cycle initiation. We identified the pilin protein PilA together with 6 additional components of a multi-layered c-di-GMP signalling network (Fig. 1) as key determinants that control cell cycle initiation. Using FRET microscopy studies, we quantified c-di-GMP signalling dynamics inside single cells and found that, besides its structural role in forming type IVb pili filaments, PilA comprises a specific input signal for activation of c-di-GMP signalling at the G1-S phase transition. Furthermore, we show genetic evidence that PilA functions upstream of the PleC-PleD two-component signalling system and present data that the monomeric PilA reservoir is sensed through a short 17 amino acid long N-terminal peptide sequence (cell cycle initiation pilin, CIP). It is remarkable that the *Caulobacter* PilA is a multi-functional protein that encodes within a 59 amino acid polypeptide a leader sequences for translocation, the CIP sequence for cell cycle signalling functions as well as structural determinants required for pili polymerization.

Caulobacter exhibits a biphasic life cycle where new-born swarmer progeny undergo an obligate differentiate into surface

attached stalked cells to initiate DNA replication. How could PilA couple cell cycle initiation to surface sensing? Type IVb pili have been shown to serve as adhesion filament as well as mechano-sensors (35–37), that upon surface contact induce the retraction of pili filaments with concomitant accumulation of monomeric PilA in the inner membrane (9). Our results from genetic dissection of PilA in conjunction with FRET microscopy to monitor c-di-GMP signalling dynamics suggest a model where high levels of PilA monomers in the inner membrane are sensed via the N-terminal CIP sequence to activate the sensor kinase PleC and promote phosphorylation of the diguanylate cyclase PleD (Fig. 3e). In such a model surface sensing by pili induces a sharp increase in intra-cellular c-di-GMP levels and activates the proteolytic clearance (18, 20) of the master regulator CtrA to initiate cell cycle progression. However, the precise structural mechanism how initial surface contact stimulates pili retraction remains an open question. In *Caulobacter*, studies showed that pili upon covalent attachment of high-molecular-weight conjugates loose their dynamic activities (9). One possibility is that upon surface contact force generation leads to structural rearrangements within the filament that locks pili in the retraction state, which in turn prevents pilus extension and reincorporation of sub-units leading to elevated PilA levels in the inner membrane.

On the level of signal integration, sensing the PilA reservoir through the bifunctional kinase/phosphatase PleC provides robust signal integration to sense surfaces. Small fluctuations in the inner membrane PilA concentrations due to dynamic pili cycling in the planktonic state do not lead to permanent increase in cellular c-di-GMP levels as PleC kinase activity induced upon retraction is reversed when pili are extended again and PleC is reset to a phosphatase. In a model where surface contact locks pili in the retraction state, the kinase activity of PleC wins the tug of war leading to a permanent increase in c-di-GMP levels and a robust surface sensing mechanism.

From an engineering perspective, coupling surface sensing via the inner membrane PilA reservoir to a c-di-GMP second-messenger cascade may provide a mechanism to couple cell cycle initiation to multiple orthogonal output functions including inhibition of flagellar motility (38), secretion of adhesive surface polysaccharides (9) and activation of stalk-cell specific transcriptional programs (24) to induce permanent surface attachment and cellular differentiation at the G1-S phase transition.

The bacterial second messenger cyclic diguanylate (c-di-GMP) is a key regulator of cellular motility, cell cycle initiation, and biofilm formation with its resultant antibiotic tolerance, which can make chronic infections difficult to treat (39–41). In our work, we show that the addition of a chemically produced CIP peptide specifically modulates the c-di-GMP signalling behaviour in cells and also has pleiotropic effects on surface adhesion and phage susceptibility in *Caulobacter*. Therefore, the CIP peptide, regulating the spatiotemporal production of c-di-GMP, might be an attractive drug target for the control of biofilm formation that is part of chronic infections. Given the broad conservation of type IV pili and their central role in human pathogens to drive infection and host colonization (42), the CIP peptide identified represents a new chemotype and is potentially developable into a chemical genetic tool to dissect c-di-GMP signalling networks and to block surface sensing in pathogens to treat bacterial infections.

Materials and Methods

Supplementary Materials and Methods include detailed descriptions of strains, media and standard growth conditions, Tn5 transposon mutagenesis, growth selection and sequencing, FRET microscopy procedures to quantify cellular c-di-GMP levels in *Caulobacter* cells, CIP peptide assay, quantification of surface attachment and phage susceptibility assays. Data SI contains the essentiality classification of each *Caulobacter* coding sequence profiled at different growth temperatures according to TnSeq measurements.

TnSeq library generation. Tn*5* hyper-saturated transposon mutant libraries in *Caulobacter* were generated as previously described (12, 13). Transposon mutant libraries were selected on rich medium (PYE) supplemented with gentamicin. Depending on the respective library, the plates were incubated at the selection temperatures of 5, 10, 25 or 30°C. As soon as colonies appeared, the selected mutant libraries were separately pooled off the plates, supplemented with 10% v/v DMSO and stored in a 96-well format at -80°C for subsequent use.

FRET microscopy. FRET imaging was performed on a Nikon Eclipse Ti-E inverted microscope with a precisExcite CoolLED light source, a Hamamatsu ORCA-ERA CCD camera, a Plan Apo λ 100x Oil Ph3 DM objective, combined with a heating unit to maintain an environmental temperature of 25°C during the imaging. Single time point acquisitions were taken under the acquisition and channel settings according to (11).

CIP Peptide Assay. The CIP peptide was ordered from Thermo Fisher Scientific GENEART (Regensburg, Germany). Stocks were kept in 100% DMSO and the peptide was applied in a final DMSO concentration of 4% to synchronized *Caulobacter* NA1000 wt and $\Delta pilA$ populations prior FRET-microscopy. The swarmer fraction was resuspended in M2 salts and the CIP peptide was administered to a final concentration of 100 uM.

ACKNOWLEDGMENTS. We thank C. Aquino and R. Schlapbach from the Zurich Functional Genomics Center for sequencing support, Y. Brun, H-M. Fischer, W-D. Hardt, S.I. Miller, L. Shapiro and J. Vorholt for helpful comments on the manuscript. This work received institutional support from the Swiss Federal Institute of Technology (ETH) Zürich, ETH research grant [ETH-08 16-1] to B.C, and the Swiss National Science Foundation, [31003A_166476, 310030_184664 and CRSII5_177164] to B.C.

1. C Berne, CK Ellison, A Ducret, YV Brun, Bacterial adhesion at the single-cell level. *Nat. Rev. Microbiol.* **16**, 616 (2018).
2. G Li, et al., Surface contact stimulates the just-in-time deployment of bacterial adhesins. *Mol. microbiology* **83**, 41–51 (2012).
3. J Palmer, S Flint, J Brooks, Bacterial cell attachment, the beginning of a biofilm. *J. industrial microbiology & biotechnology* **34**, 577–588 (2007).
4. CS Smith, A Hinz, D Bodenmiller, DE Larson, YV Brun, Identification of genes required for synthesis of the adhesive holdfast in caulobacter crescentus. *J. bacteriology* **185**, 1432–1442 (2003).
5. L Shapiro, Differentiation in the caulobacter cell cycle. *Annu. review microbiology* **30**, 377–407 (1976).
6. PD Curtis, YV Brun, Getting in the loop: regulation of development in caulobacter crescentus. *Microbiol. Mol. Biol. Rev.* **74**, 13–41 (2010).
7. HH McAdams, L Shapiro, The architecture and conservation pattern of whole-cell control circuitry. *J. Mol. Biol.* **409**, 28–35 (2011).
8. M Brilli, et al., The diversity and evolution of cell cycle regulation in alpha-proteobacteria: a comparative genomic analysis. *BMC Syst. Biol.* **4**, 1–16 (2010).
9. CK Ellison, et al., Obstruction of pilus retraction stimulates bacterial surface sensing. *Science* **358**, 535–538 (2017).
10. I Hug, S Deshpande, KS Sprecher, T Pfohl, U Jenal, Second messenger–mediated tactile response by a bacterial rotary motor. *Science* **358**, 531–534 (2017).
11. M Christen, et al., Asymmetrical Distribution of the Second Messenger c-di-GMP upon Bacterial Cell Division. *Science* **328**, 1295–1297 (2010).
12. B Christen, et al., The essential genome of a bacterium. *Mol. Syst. Biol.* **7**, 528 (2011).
13. M Christen, et al., Quantitative Selection Analysis of Bacteriophage ϕCbK Susceptibility in Caulobacter crescentus. *J. Mol. Biol.* **428**, 419–430 (2016).
14. B Zhou, et al., The Global Regulatory Architecture of Transcription during the Caulobacter Cell Cycle. *PLoS Genet.* **11**, e1004831 (2015).
15. JM Schrader, et al., Dynamic translation regulation in caulobacter cell cycle control. *Proc. Natl. Acad. Sci.* **113**, E6859–E6867 (2016).
16. M Kanehisa, M Furumichi, M Tanabe, Y Sato, K Morishima, KEGG: new perspectives on genomes, pathways, diseases and drugs. *Nucleic Acids Res.* **45**, D353–D361 (2016).
17. B Christen, et al., High-throughput identification of protein localization dependency networks. *Proc. Natl. Acad. Sci.* **107**, 4681–4686 (2010).

18. SC Smith, et al., Cell cycle-dependent adaptor complex for clpxp-mediated proteolysis directly integrates phosphorylation and second messenger signals. *Proc. Natl. Acad. Sci.* **111**, 14229–14234 (2014).
19. AA Iniesta, PT McGrath, A Reisenauer, HH McAdams, L Shapiro, A phospho-signaling pathway controls the localization and activity of a protease complex critical for bacterial cell cycle progression. *Proc. Natl. Acad. Sci.* **103**, 10935–10940 (2006).
20. A Duerig, et al., Second messenger-mediated spatiotemporal control of protein degradation regulates bacterial cell cycle progression. *Genes & development* **23**, 93–104 (2009).
21. R Wright, C Stephens, G Zweiger, L Shapiro, M Alley, Caulobacter lon protease has a critical role in cell-cycle control of dna methylation. *Genes & development* **10**, 1532–1542 (1996).
22. K Jonas, J Liu, P Chien, MT Laub, Proteotoxic stress induces a cell-cycle arrest by stimulating lon to degrade the replication initiator dnaa. *Cell* **154**, 623–636 (2013).
23. KG Gora, et al., Regulated proteolysis of a transcription factor complex is critical to cell cycle progression in c aulobacter crescentus. *Mol. microbiology* **87**, 1277–1289 (2013).
24. A Kaczmarczyk, et al., Precise transcription timing by a second-messenger drives a bacterial g1/s cell cycle transition. *bioRxiv*, 675330 (2019).
25. E Trampari, et al., Bacterial rotary export atpases are allosterically regulated by the nucleotide second messenger cyclic-di-gmp. *J. Biol. Chem.* **290**, 24470–24483 (2015).
26. P Wassmann, et al., Structure of bef3–modified response regulator pled: implications for diguanylate cyclase activation, catalysis, and feedback inhibition. *Structure* **15**, 915–927 (2007).
27. PH Viollier, N Sternheim, L Shapiro, A dynamically localized histidine kinase controls the asymmetric distribution of polar pili proteins. *The EMBO J.* **21**, 4420–4428 (2002).
28. R Paul, et al., Allosteric regulation of histidine kinases by their cognate response regulator determines cell fate. *Cell* **133**, 452–461 (2008).
29. M Tomich, DH Fine, DH Figurski, The TadV Protein of Actinobacillus actinomycetemcomitans Is a Novel Aspartic Acid Prepilin Peptidase Required for Maturation of the Flp1 Pilin and TadE and TadF Pseudopilins. *J. Bacteriol.* **188**, 6899–6914 (2006).
30. CL Giltner, Y Nguyen, LL Burrows, Type IV Pilin Proteins: Versatile Molecular Modules. *Microbiol. Mol. Biol. Rev.* **76**, 740–772 (2012).
31. J Mignolet, G Panis, PH Viollier, More than a Tad: spatiotemporal control of Caulobacter pili. *Curr. Opin. Microbiol.* **42**, 79–86 (2018).
32. L Craig, KT Forest, B Maier, Type IV pili: dynamics, biophysics and functional consequences. *Nat. Rev. Microbiol.* **17** (2019).
33. P Entcheva-Dimitrov, AM Spormann, Dynamics and Control of Biofilms of the Oligotrophic Bacterium Caulobacter crescentus. *J. Bacteriol.* **186**, 8254–8266 (2004).
34. SP Wang, PL Sharma, PV Schoenlein, B Ely, A histidine protein kinase is involved in polar organelle development in caulobacter crescentus. *Proc. Natl. Acad. Sci.* **90**, 630–634 (1993).
35. L Craig, KT Forest, B Maier, Type iv pili: dynamics, biophysics and functional consequences. *Nat. Rev. Microbiol.*, 1 (2019).
36. CA Rodesney, et al., Mechanosensing of shear by pseudomonas aeruginosa leads to increased levels of the cyclic-di-gmp signal initiating biofilm development. *Proc. Natl. Acad. Sci.* **114**, 5906–5911 (2017).
37. YF Inclan, et al., A scaffold protein connects type iv pili with the chp chemosensory system to mediate activation of virulence signaling in pseudomonas aeruginosa. *Mol. microbiology* **101**, 590–605 (2016).
38. M Christen, et al., Dgra is a member of a new family of cyclic diguanosine monophosphate receptors and controls flagellar motor function in caulobacter crescentus. *Proc. Natl. Acad. Sci.* **104**, 4112–4117 (2007).
39. U Römling, M Gomelsky, MY Galperin, C-di-gmp: the dawning of a novel bacterial signalling system. *Mol. microbiology* **57**, 629–639 (2005).
40. LR Hoffman, et al., Aminoglycoside antibiotics induce bacterial biofilm formation. *Nature* **436**, 1171 (2005).
41. PA Cotter, S Stibitz, c-di-gmp-mediated regulation of virulence and biofilm formation. *Curr. opinion microbiology* **10**, 17–23 (2007).
42. AJ Merz, CA Enns, M So, Type iv pili of pathogenic neisseriae elicit cortical plaque formation in epithelial cells. *Mol. microbiology* **32**, 1316–1332 (1999).

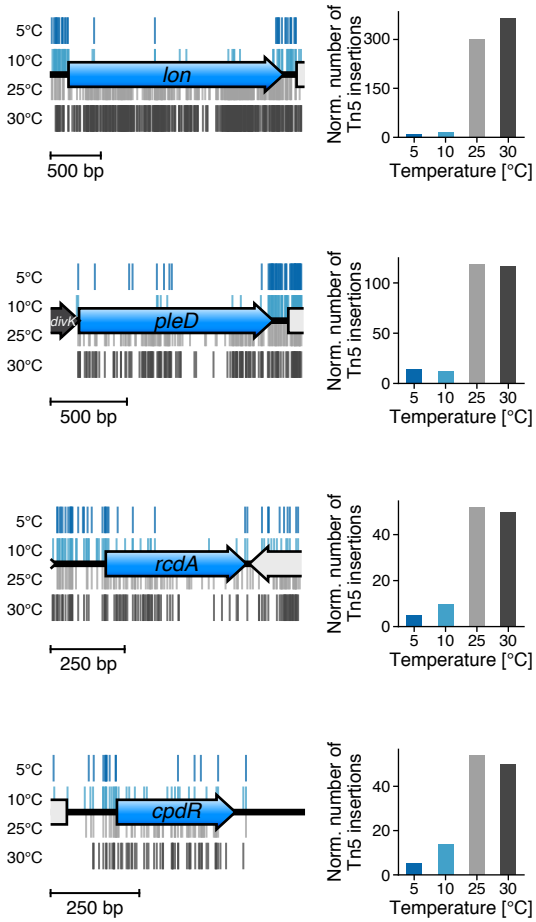

Fig. S1. Tn*5* insertion patterns and numbers of insertions in conditional essential cell cycle genes of cluster A required for slow growth (blue arrows). The genomic positions of transposon insertions recovered upon selection a the respective growth temperature are plotted above and below the genome track as blue to dark grey marks. The normalized number of insertions within the open reading frame are plotted on the right.

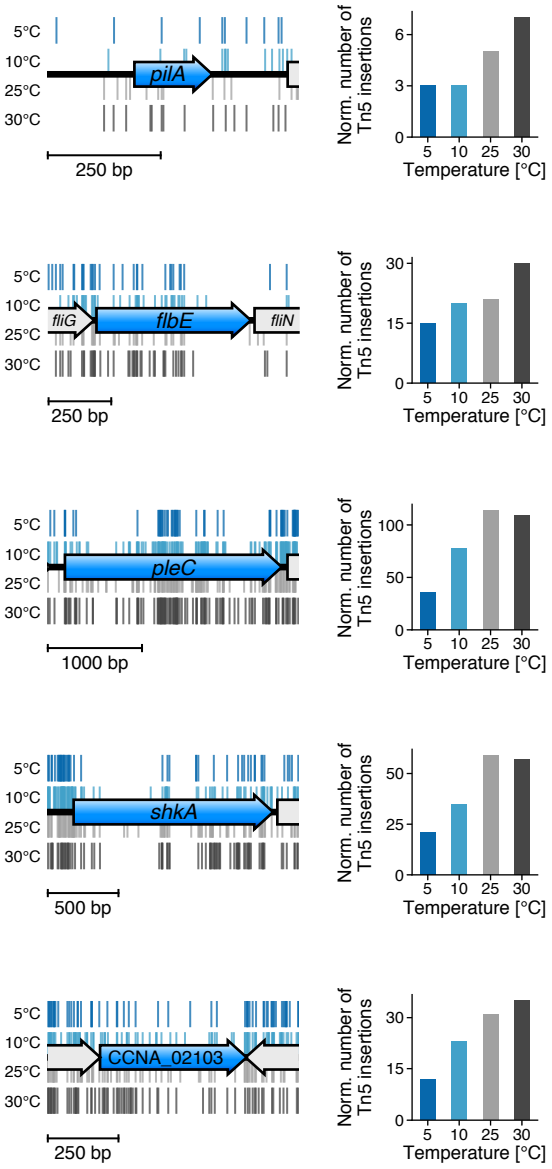

Fig. S2. Tn*5* insertion patterns and numbers of insertions in conditional essential cell cycle genes of cluster B required for slow growth (blue arrows). The genomic positions of transposon insertions recovered upon selection a the respective growth temperature are plotted above and below the genome track as blue to dark grey marks. The normalized number of insertions within the open reading frame are plotted on the right.

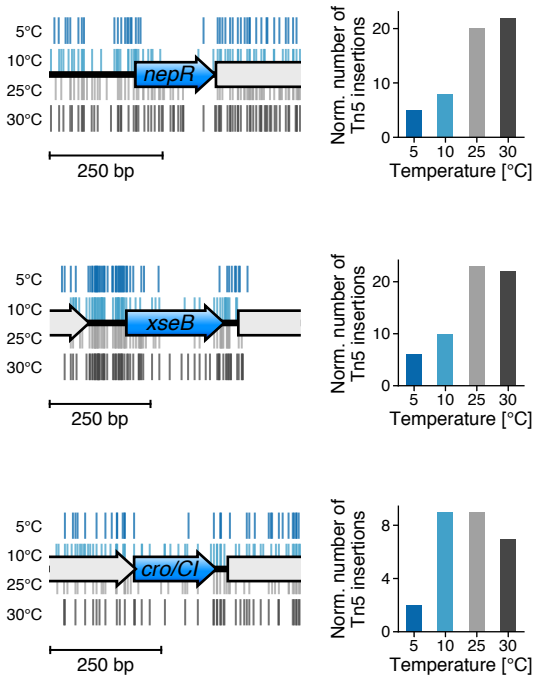

Fig. S3. Tn*5* insertion patterns and numbers of insertions in conditional essential cell cycle genes of cluster C required for slow growth (blue arrows). The genomic positions of transposon insertions recovered upon selection a the respective growth temperature are plotted above and below the genome track as blue to dark grey marks. The normalized number of insertions within the open reading frame are plotted on the right.

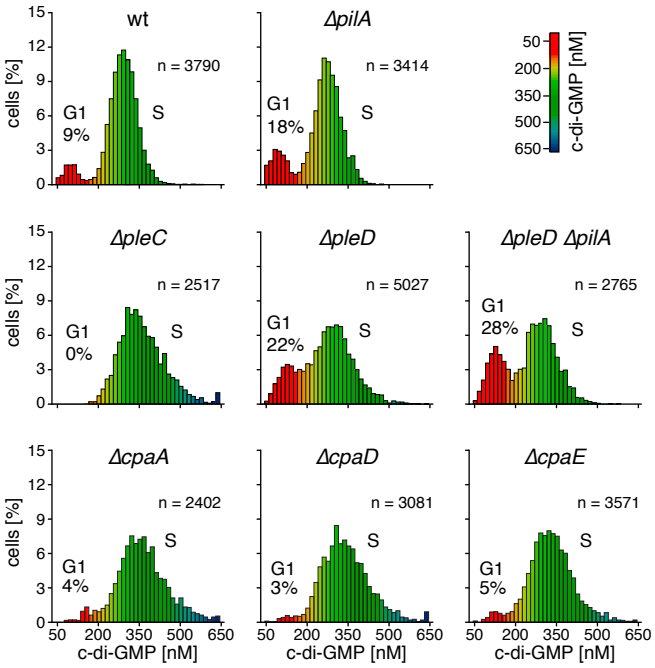

Fig. S4. Population distribution of intra-cellular c-di-GMP concentrations in *Caulobacter* cells assessed by time-lapse FRET microscopy. Cells with low c-di-GMP levels correspond to swarmer cells (G1) while cells with high c-di-GMP concentrations correspond to replication competent stalked cells (S).

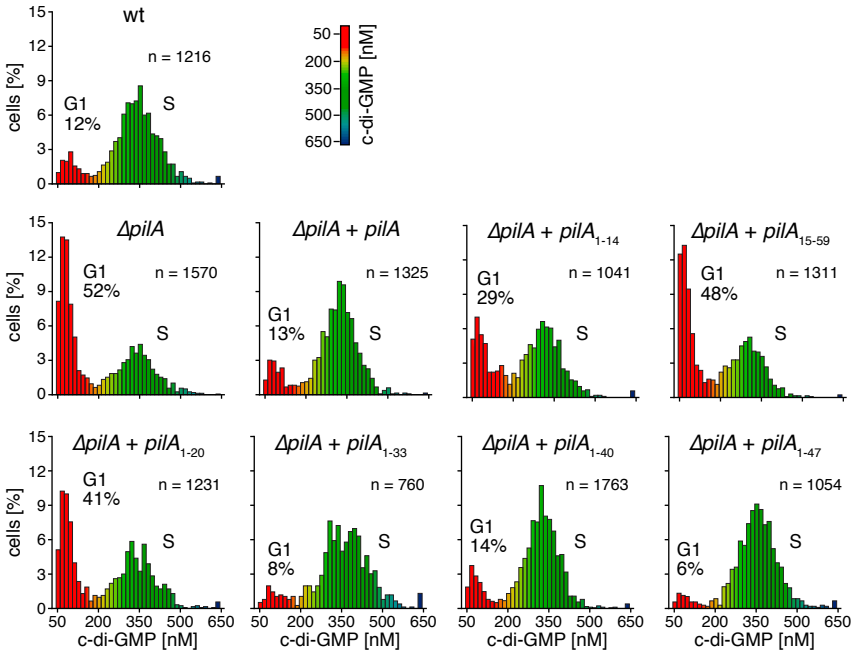

Fig. S5. Population distribution of intra-cellular c-di-GMP concentrations in synchronized *Caulobacter* cells with different *pilA* backgrounds assessed by FRET microscopy. Cells with low c-di-GMP levels correspond to swarmer cells (G1) while cells with high c-di-GMP concentrations correspond to replication competent stalked cells (S).

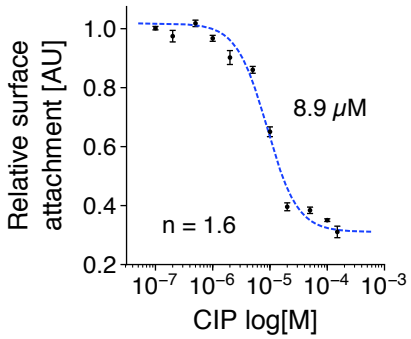

Fig. S6. Concentration response curve of the CIP peptide inhibiting cellular attachment with a EC_{50} of 8.9 and a hill coefficient of 1.6.

Table S1. Minimal generation times of *Caulobacter* in PYE medium at selected growth temperatures.

Growth temperature [°C]	Generation time [h]
5	52.6[a]
10	18.2 ± 0.24
25	1.7 ± 0.04
30	1.4 ± 0.02

[a] Calculated generation time according to Ratkowsky form.

Table S2. Transposon sequencing statistics

Tn5 mutant library	Mapped reads[a]	Unique Tn5 insertions[b]	Mean gap [bp][c]	Median gap [bp][c]
5 ℃	7'838'227	398'150	10	5
10 ℃	9'726'083	502'774	8	4
25 ℃	9'773'590	397'377	10	5
30 ℃	10'380'804	399'751	10	5

[a] Number of unambiguously mapped paired-end reads.
[b] Number of unique transposon insertions mapped.
[c] Gap between consecutive transposon insertions.

Table S3. Complementation analysis of PilA variants and distribution of cell cycle states according to single cell c-di-GMP measurement.

Genotype	G1 phase [n cells]	S phase [n cells]	Fraction in G1 phase [%]	P-value[a]
wt	143	1073	11.76	-
Δ*pilA*	821	749	52.29	$4.96 \cdot 10^{-119}$
Δ*pilA* + *pilA*	174	1151	13.13	$3.07 \cdot 10^{-1}$
Δ*pilA* + $pilA_{1\text{-}14}$	304	737	29.20	$3.60 \cdot 10^{-25}$
Δ*pilA* + $pilA_{15\text{-}59}$	623	688	47.52	$5.83 \cdot 10^{-90}$
Δ*pilA* + $pilA_{1\text{-}20}$	499	732	40.54	$2.71 \cdot 10^{-61}$
Δ*pilA* + $pilA_{1\text{-}33}$	62	698	8.16	$1.20 \cdot 10^{-3}$
Δ*pilA* + $pilA_{1\text{-}40}$	241	1522	13.67	$1.33 \cdot 10^{-1}$
Δ*pilA* + $pilA_{1\text{-}47}$	59	995	5.60	$1.20 \cdot 10^{-7}$

[a] Fisher's exact test of observing the measured population distribution under the null hypothesis that cell cycle states are distributed as in the wt.

Table S4. Essentiality of the pilus assembly genes within the Tad locus.

Locus_tag	Gene	Functional annotation	Essentiality
CCNA_03043	*pilA*	type IVb pilin protein	essential for slow growth
CCNA_03042	*cpaA*	Prepilin peptidase	non-essential
CCNA_03041	*cpaB*	Periplasmic pilus assembly subunit	non-essential
CCNA_03040	*cpaC*	Outer membrane pilus secretion channel	non-essential
CCNA_03039	*cpaD*	Periplasmic pilus assembly subunit	non-essential
CCNA_03038	*cpaE*	Pilus assembly ATPase	non-essential
CCNA_03037	*cpaF*	Extension and Retraction ATPase	non-essential
CCNA_03036	*cpaG*	TadB-related pilus assembly protein	non-essential
CCNA_03035	*cpaH*	TadC-related pilus assembly protein	non-essential
CCNA_03044	*cpaI*	CpaC-related secretion pathway protein	non-essential
CCNA_03045	*cpaJ*	Pseudopilin	non-essential
CCNA_03046	*cpaK*	Pseudopilin	non-essential

Supplementary Information for

The type IV pilin PilA couples surface attachment and cell cycle initiation in *Caulobacter crescentus*

Luca Del Medico, Dario Cerletti, Matthias Christen, and Beat Christen

E-mail: matthias.christen@imsb.biol.ethz.ch, beat.christen@imsb.biol.ethz.ch

This PDF file includes:

Supplementary text
Caption for Database S1
References for SI reference citations

Other supplementary materials for this manuscript include the following:

Database S1

Supporting Information Text

Supplementary Materials & Methods

(i) Bacterial strains and growth conditions.

Strains, media and standard growth conditions. *Caulobacter crescentus* was cultivated on liquid and solid Peptone-yeast (PYE) at 30°C. *Escherichia coli* was cultivated on liquid and solid Luria-Bertani (LB) broth at 37°C. If necessary, the media were supplemented with 0.1% xylose and/or antibiotics at the following concentrations: gentamycin: 2.5 µg/ml (PYE liquid medium), 10 µg/ml (PYE agar), and 15 µg/ml (LB agar); nalidixic acid: 20 µg/ml, (PYE agar); ampicillin 50 µg/ml (PYE agar), oxytetracycline 2.5 µg/ml (PYE liquid medium), 10 µg/ml (PYE agar), tetracycline 12 µg/ml (LB liquid medium), 10 µg/ml (LB agar).

Determination of growth rates. Growth rates at temperature 30°C were determined on a TECAN Infinite® M200 multimode reader in a randomized 96-well format. 10 replicates were measured, each in 200 µl PYE. The OD_{600} was measured at 10 min intervals over 23 h with shaking between measurements at an amplitude of 5 mm. Similarly, the determination of the growth rate at temperatures 25°C and below were performed by measuring the OD_{600} of triplicate *Caulobacter* cultures grown in 50 ml PYE in 250 Erlenmeyer flasks at 250 rpm. The OD_{600} measurements were taken in 30 to 60 min intervals on a TECAN Sunrise® plate reader. Growth rates were calculated according to the bacterial exponential growth model. The growth rate at 5°C was inferred by the Ratkowsky form (1), $r \sim (T - T_0)^2$, fitted over the growth temperature range 10 - 35°C.

Determination of Cell Cycle Phase. To determine the population proportions of *Caulobacter* cells in the swarmer (G1 phase) and replicative (S phases), a *Caulobacter* strain bearing fluorescent cell cycle markers (2)(*divJ::rfp*, *pleC::mYPet*, *mCYPet::cpaE*), was grown to mid-exponential phase in PYE medium at 10°C and 30°C. The cells were imaged on agarose pads with a Nikon Eclipse Ti-E inverted microscope at a 100x magnification equipped with a precisExcite CoolLED light-source and a Hamamatsu ORCA-ERA CCD camera. The classification into swarmer and replicative cell cycle states was performed according to the fluorescent markers displayed in the different cell cycle states as previously described (2). Cells with polar localized PleC-mYPet markers (G1 phase) were classified as swarmer cells and cells with polar localized DivJ-RFP markers were classified as stalked cells (S-phase).

Synchronization of Caulobacter cultures. *Caulobacter* was synchronized (3) by harvesting in mid-log phase and pelleting at 6000 rpm for 10 min at 4°C. The pellet was resuspended in 1 ml of ice-cold M2 medium, again centrifuged at 13000 rpm at 4°C prior resuspending the cell pellet in 900 µl M2 and 900 µl of Percoll™ (Sigma-Aldrich CHEMIE Gmbh, Germany). The sample was centrifuged for 20 min at 11000 rpm at 4°C. The top stalk cell band was aspirated off and the lower swarmer band collected. The swarmer fraction was then washed twice in 1 ml ice-cold M2 and resuspended in the appropriate medium.

(ii) Transposon mutagenesis, growth selection and sequencing.

Tn5 Transposon mutagenesis and temperature selection. Hypersaturated transposon mutagenesis libraries were generated as previously described (4, 5). In short, a separate transposon mutant library was generated for each temperature selection by conjugating a barcoded Tn*5* derivative from an *E. coli* S17-1 delivery strain into the wt *Caulobacter* NA1000 recipient strain. The conjugations were performed on 0.45 µm membrane filters followed by a 30°C overnight incubation on PYE plates . Cells from each filter were resuspended in 450 µl PYE and plated in 50 µl aliquots onto selective PYE plates supplemented with xylose, gentamycin and nalidixic acid plates. Depending on the respective library, the plates were incubated at the selection temperatures of 5, 10, 25 or 30°C. As soon as colonies appeared, the selected mutant libraries were separately pooled off the plates, supplemented with 10% v/v DMSO and stored in a 96-well format at -80°C for later use.

DNA extraction and parallel PCR amplification of transposon junctions. Genomic DNA aliquots of each mutant library were isolated in 96-well format by repeated heat shock and snap freeze cycles taking 100 µl aliquots per library well. Five repeated heat and snap freeze cycles were conducted in a 96-well PCR plate with 5 min boiling at 95°C directly followed by snap freezing the samples in liquid nitrogen. The transposon junctions were amplified from the genomic DNA samples as previously described (4, 5). The two-step semi-arbitrary PCR reaction were performed in 10 µl volumes in 384-well PCR plates on BioRad S1000TM (Cressier, Switzerland) thermocycler instruments using GoTaq® G2 Green Master Mix (Promega, USA). In the first PCR round, 1 µl of the extracted DNA served as a reaction template per well. Each DNA template pool was independently amplified four times with the transposon specific primer (M13) and one out of four semi-arbitrary primers ensuring genomic coverage, as previously described (4). The first PCR amplification protocol consisted of: (1) 94°C for 3 min, (2) 94°C for 30 s, (3) 42°C for 30 s, slope -1°C/cycle, (4) 72°C for 1 min, (5) repeat steps 2-4, 6 times, (6) 94°C for 30 s, (7) 58°C for 30 s, (8) 72°C for 1 min, (9) repeat steps 6-8, 25 times, (10) 72°C for 1 min, (11) 12°C hold. 1 µl of the first-round PCR products were then amplified in the second nested PCR step using the Illumina paired-end primers PE1.0 and PE2.0 with the following protocol: (1) 94°C for 3 min, (2) 94°C for 30 s, (3) 64°C for 30 s, (4) 72°C for 1 min, (5) repeat steps 2-4, 30 times, (6) 72°C for 3 min, (7) 12°C hold.

DNA library preparation and sequencing of transposon junctions. The second-round PCR products of each library were pooled and size selected on a 2% agarose gel. Amplification products of 200-700 bp were selected and purified over column (Machery-Nagel, Switzerland). Of each product pool the DNA concentration was quantified on a Nanodrop ND-1000 spectrometer. All samples were paired-end sequenced (2x 125 bases) on the HiSeq Illumina platform using the Illumina sequencing chemistry version

v4 and the Illumina sequencing primers PE1.0 and PE2.0. Standard base calling was performed from raw images using a phiX reference spike-in according to the Illumina genome analyzer software suite OLB. The sequencing was performed at the Functional Genomics Center Zürich, Zürich, Switzerland.

(iii) Transposon sequencing data processing and essentiality analysis.

Raw read processing and genomic mapping of transposon insertion sites. Raw read processing and genomic sequence alignment were performed as previously described (5). Low quality reads as indicated by low phred scores were filtered and only reads containing a perfect 15 bp long match to the Tn5 end [GTGTATAAGAGACAG] and bearing genomic inserts larger than 15bp were selected. The adapters corresponding to Tn5 transposon end sequence, illumina adapters and arbitrary PCR primer sequence were trimmed. The de-multiplexing into the different experiments was performed according to the 14 bp long transposon internal barcode sequence and reads were aligned onto the *Caulobacter* NA1000 reference genome NCBI Ref. Seq.: NC_011916.1 (6)) using bwa-07.12 (7). Only reads with proper paired-end alignment and zero mismatches within the first 15 bp were kept. Furthermore, only reads with at least one of the paired-end reads mapping unambiguously to the genome and harboring a genomic insert size of fewer than 500 bases were further retrieved. The location of a given Tn*5* insertion was defined as the first genome position of the first reference base detected immediately after the transposon I-end, whereby the 9 bp long target DNA duplication upon Tn*5* insertion (8) was taken into account. Finally, global insertion statistics and insertion occurrences in annotated GenBank features (6) were calculated according to previously described metrics and routines (5).

Essentiality Analysis and Fitness Quantification. Annotated coding sequences (CDS) on the NC_011916.1 reference genome were classified into the categories essential, semi-essential, and non-essential according to metrics and statistical analyses previously used and defined (4, 5). A CDS was classified as essential if their non-disruptable 5' portion covered more than 60% of the total open reading frame. In order to include essential CDS with potential mis-annotated translational start codons, CDS were classified as essential if the transposon insertion density was less than six times the average insertion density measured across the genome and had either a single transposon insertion gap covering more than 60% of the CDS or had two significant Tn gaps together covering more than 80% of the CDS. If the average Tn density was less than four times the average insertion density across the genome but no essentiality criterion was satisfied, CDS were classified as semi-essential.

(iv) Analysis on cell cycle genes.

Extracting cell cycle genes. Cell cycle genes were defined as exhibiting cell cycle dependent transcription and translation. First, transcriptional patterns across *Caulobacter* genes were retrieved from a comprehensive data set systematically mapping the expression from transcription start sites (TSS) across the cell cycle (9). The expression profile of genes with more than one primary cell cycle regulated TSS were summed. TSS and the associated genes which could not be assigned to a cell cycle phase were excluded from the analysis. In addition, a minimal TSS expression level threshold of 30, which had to be reached at least once during the cell cycle, was set. Genes belonging to an operon controlled by one or several cell cycle regulated primary TSSs were included in the analysis if they were found downstream of the respective TSS. The *Caulobacter* (NC_011916.1) operon assignments were retrieved from the DOOR 2.0 database (10). Second, genes exhibiting a cell cycle dependent translation were retrieved from a comprehensive ribosomal profiling data set across the *Caulobacter* cell cycle (11). Genes being present in both data sets were defined as cell cycle regulated genes.

Classification of cell cycle regulated genes. All isolated cell cycle regulated genes were classified into the following growth essentiality categories: non-essential, core essential and conditional essential for slow growth. The classification was performed according to the following criteria: non-essential; a gene is non-essential across all conditions tested, core essential; a gene is essential or semi-essential at low temperatures (5 and/or 10°C) and essential or semi-essential at high temperatures (25 and/or 30°C), conditional essential for slow growth; a gene is only essential or semi-essential at low temperatures (5 and/or 10°C).

(v) c-di-GMP FRET microscopy and cell cycle state classification.

FRET imaging. In vivo c-di-GMP concentrations were quantified using a previously described genetically encoded c-di-GMP FRET sensor containing (12). *Caulobacter* NA1000 bearing the FRET sensor containing plasmid pMXMCS2::synthSpy2 was grown in M2X minimal medium supplemented with 10% PYE. For single time point imaging, cells were taken at mid-exponential phase and imaged on 2% agarose pads (h = 0.75 mm, r = 2.5 mm) placed on standard microscopy slides covered by a cover slide and sealed with araldite glue. In the case of synchronized swarmer populations, cells were resuspended in M2 salts and imaged 5 min after synchronization. For time-lapse FRET imaging, *Caulobacter* cells were taken at an $OD_{600} = 0.1$ and placed and incubated on agarose pads containing M2X with 10% PYE. Automated image aquisition was then conducted in 10 min intervals.

FRET imaging was performed on a Nikon Eclipse Ti-E inverted microscope with a precisExcite CoolLED light source, a Hamamatsu ORCA-ERA CCD camera, a Plan Apo λ 100x Oil Ph3 DM objective, combined with a heating unit to maintain an environmental temperature of 25°C during the imaging. Single time point acquisitions were taken under the acquisition and channel settings detailed in Christen et al. 2010 (12).

Image processing and FRET and c-di-GMP signal quantification. The Nikon .nd2 image frames were converted to channel separated .tiff files using the Bio-Formats (13) command line tool bfconvert (version 5.8.2) under default conversion parameters. Cell segmentation, background correction, and the extraction of the fluorescent signal per cell were performed on the converted .tiff files in the software suite oufti (version 1.0.0) (14). Background correction and the fluorescent signal extraction were performed under the default settings of version 1.0.0. To exclude mis-segmented or defective cells from the further analysis cells whose dimensions exceeded the population means in cell length and/or width by more than three standard deviations were excluded from all further analysis. Next, the fluorescent signals from both channels were separately integrated across each cell. The FRET emission ratio was calculated by dividing the integrated YFP by the integrated CFP signal, resulting in an averaged FRET emission value per cell. C-di-GMP concentrations were directly inferred according to previously established FRET ratiometric standards (12).Single cells were classified into the G1 and S phase according to the quantified c-di-GMP concentration, whereby c-di-GMP concentrations across a population were bi-modal distributed with low and high c-di-GMP concentrations corresponding to cells in the G1 and S phase, respectively (12).

(vi) Identification of the PilA signaling portion.

Construction of the pilA complementation constructs. All PilA complementation variants were expressed on a pMR20 (tet^R) plasmid in *Caulobacter* NA1000 *ΔpilA* harboring the FRET sensor pMXMCS2::synthSpy2 (kan^R) plasmid. The PilA variants were constructed by PCR amplifying the respective portion of the *pilA* (CCNA_03043) genomic locus. All variants were fused to the native *pilA* promoter sequence. The promoter and *pilA* variants were, subsequently, Gibson assembled into a BamHI digested pMR20 (tet^R) vector and electroporated into *E. coli* DH10B. The plasmids were conjugated from *E. coli* DH10B strain into *Caulobacter* NA1000 Δ*pilA* via tri-parential matings. Complementation phenotypes of PilA variants were assessed by quantifying c-di-GMP signaling states using FRET microscopy. Complementation strains were synchronized prior imaging and the c-di-GMP concentration within individual cells was determined as described above.

(vii) CIP peptide.

CIP Peptide Assay. The CIP peptide was ordered from Thermo Fisher Scientific GENEART (Regensburg, Germany). Stocks were kept in 100% DMSO and the peptide was applied in a final DMSO concentration of 4%.*Caulobacter* NA1000 wt and *ΔpilA* populations were synchronized as described above. The swarmer fraction was resuspended in M2 salts as above and the peptide administered to a final concentration of 100 uM. The peptide supplemented cultures and the corresponding control were then incubated for 15 min at RT. Following the incubation, the FRET measurements were performed as in the non-supplemented reference conditions described above.

Surface attachment assays. *Caulobacter* CB15 at an OD_{600} of 0.25 grown in PYE was transferred in 100 µl aliquots to Nunclon™ Delta Surface microwell plates (Thermo Fisher Scientific Nunc A/S, Denmark). The CIP peptide was then supplemented to the appropriate final concentration followed by incubation at 30°C for 1 h without shaking. After 1 h, the cells and medium were removed and each well gently washed 3x with dH_2O. Surface attached cells were stained with crystal violet for 15 min at RT. The supernatant was removed and each well was again gently washed 3x with dH_2O. The remaining stain on the surface attached cells was dissolved in 70% EtOH and the level of surface attachment was measured as the absorbance at A_{595} on a Tecan Sunrise plate reader.

Pili retraction assay. The induction of pili retraction in the presence of CIP peptide was assayed in *Caulobacter* NA1000 by quantifying the susceptibility towards the pili-trophic phage ΦCbk. An aliquot of a mid-log *Caulobacter* culture at (OD_{600} = 0.24) was incubated with the CIP peptide at a final concentration of 100 µM for 10 min at RT. Next, bacteriophage ΦCbk from a 10^7 stock was added and incubated for 3 min at RT. To stop the infection and wash off unattached phage particles, PYE was added in excess and the cells pelleted at 13,000 g for 2 min, followed by 3 x washing with H_2O. The last washing supernatant was kept as a negative control. The pellet was resuspended in 200 µl of the original *Caulobacter* culture in a 10^{-1} and 10^{-2} dilution, mixed with 5 ml 0.45% soft-agar, plated onto PYE agar, and incubated O/N at 30°C. The retraction of pili was then quantified by counting PFUs in the CIP treated versus untreated population.

(ix) General data analysis. Data analysis and visualization was performed in the Python programming language (version 3.5 - 3.7.3) using the open source libraries and frameworks: NumPy (15) (version 1.15.2), SciPy (16) (version 1.1.0), Pandas (17) (version 0.23.4), Matplotlib (18) (version 3.0.1), scikit-learn (19) (version 0.20.0), scikit-image (20) (version 0.14.1), Jupyter (21) (version 1.0.0). Image analysis was performed using Fiji/ImageJ (22) (version 2.0.0).

Additional data table S1 (Data_SI.xlsx)

Essentiality analysis on the cell cycle genes across the growth selections.

References

1. DA Ratkowsky, J Olley, TA McMeekin, A Ball, Relationship between temperature and growth rate of bacterial cultures. *Journal Bacteriology* **149**, 1–5 (1982).
2. B Christen, et al., High-throughput identification of protein localization dependency networks. *Proceedings National Academy Sciences* **107**, 4681–4686 (2010).
3. JW Tsai, MRK Alley, Proteolysis of the Caulobacter McpA chemoreceptor is cell cycle regulated by a ClpX-dependent pathway. *Journal Bacteriology* **183**, 5001–5007 (2001).
4. B Christen, et al., The essential genome of a bacterium. *Molecular Systems Biology* **7**, 528 (2011).
5. M Christen, et al., Quantitative selection analysis of bacteriophage ϕCbK susceptibility in Caulobacter crescentus. *Journal Molecular Biology* **428**, 419–430 (2016).
6. ME Marks, et al., The genetic basis of laboratory adaptation in Caulobacter crescentus. *Journal Bacteriology* **192**, 3678–3688 (2010).
7. H Li, R Durbin, Fast and accurate long-read alignment with Burrows–Wheeler transform. *Bioinformatics* **26**, 589–595 (2010).
8. WS Reznikoff, Transposon Tn5. *Annual Review Genetics* **42**, 269–286 (2008).
9. B Zhou, et al., The global regulatory architecture of transcription during the Caulobacter cell cycle. *PLoS Genetics* **11**, e1004831 (2015).
10. X Mao, et al., DOOR 2.0: presenting operons and their functions through dynamic and integrated views. *Nucleic Acids Research* **42**, D654–D659 (2013).
11. JM Schrader, et al., Dynamic translation regulation in Caulobacter cell cycle control. *Proceedings National Academy Sciences United States America* **113**, E6859–E6867 (2016).
12. M Christen, et al., Asymmetrical distribution of the second messenger c-di-GMP upon bacterial cell division. *Science* **328**, 1295–1297 (2010).
13. M Linkert, et al., Metadata matters: access to image data in the real world. *The Journal Cell Biology* **189**, 777–782 (2010).
14. A Paintdakhi, et al., Oufti: an integrated software package for high-accuracy, high-throughput quantitative microscopy analysis. *Molecular Microbiology* **99**, 767–777 (2015).
15. S van der Walt, SC Colbert, G Varoquaux, The NumPy array: a structure for efficient numerical computation. *Computing Science & Engineering* **13**, 22–30 (2011).
16. E Jones, T Oliphant, P Peterson, et al., SciPy: Open source scientific tools for Python (2001 –) "http://www.scipy.org/".
17. W McKinney, Data structures for statistical computing in Python in *Proceedings of the 9th Python in Science Conference*, eds. S van der Walt, J Millman. pp. 51–56 (2010).
18. JD Hunter, Matplotlib: A 2D Graphics Environment. *Computing Science & Engineering* **9**, 90–95 (2007).
19. F Pedregosa, et al., Scikit-learn: machine learning in Python. *J. Mach. Learn. Res.* **12**, 2825–2830 (2011).
20. S van der Walt, et al., scikit-image: image processing in Python. *PeerJ* **2**, e453 (2014).
21. T Kluyver, et al., Jupyter Notebooks-a publishing format for reproducible computational workflows. in *ELPUB*. pp. 87–90 (2016).
22. J Schindelin, et al., Fiji: an open-source platform for biological-image analysis. *Nature Methods* **9**, 676 (2012).